2021 IEEE International Geoscience and Remote Sensing Symposium IGARSS, 2021.
ISBN:978-1-6654-0369-6, Electronic ISSN: 2153-7003.
Pages 1634-1637
July 2021,
https://doi.org/10.1109/IGARSS47720.2021.9553166
https://archimer.ifremer.fr/doc/00757/86879/

Ku-band Polarization Difference Model for the Scatterometer Wind Inversion

Mironov Alexey [1, *], Quilfen Yves [2], Chapron Bertrand [2], Kudryavtsev V.N. [3]

[1] eOdyn, Plouzané, France
[2] Laboratory for Ocean Physics and Satellite Remote Sensing, IFREMER, Plouzané, France
[3] Satellite Ocean Laboratory, Russian State Hydrometeorological University, St. Petersburg, Russia

* Corresponding author : Alexey Mironov, email address : alexey.mironov@eodyn.com

Abstract :

The CFOSAT mission provides a unique data set of collocated nadir, near-nadir and moderate angle dual-polarization Ku-band radar measurements. These combined measurements open new opportunities to revisit existing interpretation and approaches to analyze ocean radar backscatter signals. In particular, actual scatterometer wind vector retrieval algorithms and definitions of Geophysical Modulation Functions (GMFs) can be revisited, including sensitivity to additional parameters: wave state, currents, etc. The present work describes an alternative GMF approach based on the analysis of signal polarization differences, and interpretation in terms of ocean surface wind-roughness spectra. Based on CFOSAT measurements, the polarization-difference GMF reproduces main properties of standard empirical radar GMFs. However, it is more directly related to a theoretical short wave spectral model. This approach naturally enables the inclusion of additional sea state variables. Results of this work is intended to be implemented in wind retrieval processors to complement existing methods.

Keywords : wind scatterometry, CFOSAT, SCAT, Ku-Band, sea surface radar backscattering, polarization difference model

I. Introduction

The scatterometer instrument (SCAT) on-board China-France Oceanography Satellite (CFOSAT) mission instrument is a Ku-band space-borne radar instrument, performing dual-polarization scatterometer measurements over a wide range of moderate incidence angles [1]. A second sensor, the wave scatterometer SWIM, operates at near-nadir incidence angles, to uniquely provide collocated estimates of directional wave spectral properties [2]. These resulting collocated data sets for wind and wave observations, and this original multi-incidence and azimuthal radar configuration, provide unique opportunities to investigate the sea state impacts on the satellite radar wind estimates. In this work, our motivation is to propose a theoretical framework to help refine the analysis of sea surface backscatter properties and to extend the wind vector inversion algorithm.

Usually, Geophysical Model Functions (GMFs) are derived to describe relationships between Normalized Radar Backscattering Cross-Section (NRSC) mean and spectral properties with ocean sea surface statistical and forcing properties. For wind scatterometry, the robust derivation of the GMF is the key element for the wind vector inversion algorithm, describing the sensitivity of the averaged NRSC properties, at each incidence and observation azimuth, with wind speed and/or direction changes. As a common practice, for each new instrument, a GMF is derived from massive collocations of radar measurements with global wind model outputs and offshore buoy network data. Very efficient, this empirical approach can still suffer to cover all environmental conditions, e.g. non-stationary sea state, sea surface current, sea surface temperature, presence of biological films, ...

For Ku-band instrument, a reference GMF is the NSCAT-4 GMF [3], [4] which directly relates NRSC with wind speed and direction as $\sigma(\theta,\phi) \propto f(\mathbf{U_{10}}(U_{10},\varphi_u))$, where θ and φ is the radar observation incidence angle and azimuth, $\mathbf{U_{10}}$ is the wind vector with wind speed U_{10} and direction φ_u. Hereafter, we propose an alternative version of GMF derivation, based on the differing polarization sensitivity of backscatter Ku-band signals. This approach is indeed anticipated to quantitatively separate the measured roughness variations between changes associated with denser breaking patches and purely resonant short-scale scatter modulations [5]. Polarization sensitivity, i.e. the difference between vertically (VV) and horizontally (HH) polarized radar signals, is indeed characteristic of a resonant scattering mechanism mostly governed by small surface scales. This strategy can then build on the use of semi-empirical short wind spectra, e.g. [6]–[8].

II. Theoretical Background

Following [9]–[11], the NRSC is represented as a sum of polarized, so-called Bragg (BR) and non-polarized (NP) components

$$\sigma^{pol} = \sigma^{pol}_{br} + \sigma^{pol}_{np}, \tag{1}$$

where ^{pol} indicates vertical (V) or horizontal (H) polarization. Assuming Gaussian distribution of tilting waves, to the second order in slopes, the NRSC is expressed as [6], [11]:

$$\sigma^{pol}_{br} = \pi G^2_{pol} B(k_{br,\varphi})(1 + g_{pol} s_i^2 + h_{pol} s_i^2), \tag{2}$$

$$g_v = \frac{1}{2G_v^2}\frac{\partial^2 G_v^2}{\partial\theta^2}, \tag{3}$$

$$g_h = \frac{1}{2G_h^2}\frac{\partial^2 G_h^2}{\partial\theta^2} + \frac{2}{\sin^2}\frac{|G_v|}{|G_h|}\frac{s_c^2}{s_i^2}, \tag{4}$$

$$h_{pol} = M_t^{pol} M_h, \tag{5}$$

$$M_t = \frac{1}{G^2_{pol}}\frac{\partial G^2_{pol}}{\partial\theta}, \tag{6}$$

where geometric scattering coefficients are

$$G_v = \frac{[\epsilon + (\epsilon - 1)\sin^2\theta](\epsilon - 1)\cot^2\theta}{(\epsilon\cos\theta + (\epsilon - \sin^2\theta)^{\frac{1}{2}})^2}, \quad (7)$$

$$G_h = \frac{(\epsilon - 1)\cot^2\theta}{(\cos\theta + (\epsilon - \sin^2\theta)^{\frac{1}{2}})^2}, \quad (8)$$

$B(k_{br}, \varphi)$ is the folded saturation spectrum at the Bragg resonant wavenumebr $k_{br} = 2k_r \sin\theta$ in the incidence plane rotated by azimuth φ from wind direction, k_r is the radar wavenumber, ϵ is the seawater complex dielectric constant, s_i^2 and s_c^2 are the mean-square slope of tilting wave in- and out-of incidence plane, M_t^{pol} and M_h are the tilt and slope correlated parts of hydrodynamics modulation transfer function respectively. Key, the unknown σ_{np} component cancels out by considering polarization difference (hereafter PD)

$$\Delta\sigma = \sigma_v - \sigma_h, \quad (9)$$

so

$$\Delta\sigma = \pi B(k_{br}, \varphi)(\Delta[G_{pol}^2(1 + g_{pol}s_i^2)] + \\ + \Delta[G_{pol}^2 h_{pol}]s_i^2]\cos\varphi), \quad (10)$$

where $\Delta[x^{pol}] = x^v - x^h$ is the PD operator.

A. Semi-Empirical Wave Model

The main unknown term in the above formulation is the saturation spectrum at Bragg wavenumber $B(k_{br}, \varphi)$. For wind speed range $3 < U_{10} < 20\,m/s$, a first guess can follow the semi-empirical short wave spectrum model formulated in [7], [8]. For wind inversion, a critical parameter is the wind exponent n, $B \propto U_{10}^n$. In [8], this parameter was adjusted to fit field measurements by [7]. It will be shown later, it also largely agrees with empirical GMF derived from SCAT measurements.

Similar to [7], the angular spreading of saturation spectrum is expressed with omni-directional saturation spectrum $B_0(k_{br}) = \int_0^{2\pi} B(k_{br}, \varphi)d\varphi$ and spectrum angular width parameter $\delta(k_{br})$, such as

$$B(k_{br}, \varphi) = B_0(k_{br})(1 + \delta\cos 2\varphi))/2\pi. \quad (11)$$

B. The Relation Between Wave Saturation Spectrum and GMF

Commonly, the GMF is expressed as a truncated Fourier serie: $\sigma \approx A_0 + A_1\cos\varphi + A_2\cos 2\varphi$. The expansion of PD gives:

$$A_0 = B_0(k_{br})\Delta[G_{pol}^2(1 + g_{pol}s_i^2)]/2, \quad (12)$$

$$A_1 = B_0(k_{br})\Delta[G_{pol}^2 h_{pol}s_i^2]/2, \quad (13)$$

$$A_2 = B_0(k_{br})\Delta[G_{pol}^2(1 + g_{pol}s_i^2)]\delta(k_{br})/2. \quad (14)$$

From the other hand, the same Fourier coefficients can be obtained directly from radar measurements [9]:

$$A_0 = (\Delta\sigma^{up} + 2\Delta\sigma^{cross} + \Delta\sigma^{down})/4, \quad (15)$$

$$A_1 = (\Delta\sigma^{up} - \Delta\sigma^{down})/2, \quad (16)$$

$$A_2 = (\Delta\sigma^{up} - 2\Delta\sigma^{cross} + \Delta\sigma^{down})/4, \quad (17)$$

where ^{up}, ^{cross}, and ^{down} correspond to up-, cross-, down-wind directions of radar observations respectively.

III. Ku-Band Radar GMFs

A. SCAT and NSCAT observations

The evaluation of PD model in the context of wind inversion problem was done with the use of SCAT 40 days observation data set and additionally with NSCAT empirical GMFs described in [3], [4], [9]. The instrumental parameters of both missions are listed in the Table I.

TABLE I
SCAT AND NSCAT INSTRUMENTAL PARAMETERS

Parameter name	***SCAT***	***NSCAT***
Frequency	13.256 GHz	13.995 GHz
Pointing inc. angle	40°	45°
Inc. angle range	26° to 52°	18° to 54°
Central k_{br}	357 rad/m	415 rad/m
k_{br} range	244 to 438 rad/m	181 to 474 rad/m
Mission dates	24-11-2018 till now	17-08-1996 to 30-06-1997
Antenna type	dual-pol. rotating	six dual-pol. fixed
Swath width	≈1100 km	two swaths, 600 km each

The SCAT radar data, related to the period of September-October 2020, was processed with conventional CFOSAT Wind Data Processor (CWDP) processor [12] using 2DVAR ambiguity removal approach [13], [14] to obtain collocated wind vectors with standard 25 km wind cell resolution. Following Eq. (15-17) the Fourier coefficients were estimated for H- and V-polarizations in the range of wind speeds 2-20 m/s and for radar incidence angle range from 30° to 50°.The same estimation of Fourier coefficients in application to NSCAT measurements was reported and discussed in [9] and can be directly compared with the present SCAT measurements.

Independently, the NSCAT-4 model was obtained and regularly revised to provide optimal performance together with existing wind inversion algorithms realization and well-established calibration and ambiguity removal procedures e.g. [15] and [12]. Note, there is only one h-polarization antenna on each side of NSCAT swath. Following [3], vertical and horizontal polarization components were thus differently derived. Strictly, NSCAT-4 may not be guaranteed to be fully consistent with the formulated PD analysis. Still, NSCAT-4 GMF is the reference model for most Ku-band scatterometer data processors, and will be used in the present analysis.

B. Radar and Theoretical Model Spectrum Properties

From empirical GMFs, an omni-directional spectral estimate at Bragg wave number can be derived from Eq. (12) using measured PD A_0 coefficients:

$$B_0(k_{br}) = \frac{2A_0}{\Delta[G_{pol}^2(1 + g_{pol}s_i^2)]}. \quad (18)$$

The Figure 1 shows $B_0(\theta, U_{10})$ estimations, using 3 different GMFs, and compared with the model [8]. The incidence angle is related to Bragg and radar microwave wave numbers as

$$\theta = \arcsin\left(\frac{k_{br}}{2k_r}\right). \quad (19)$$

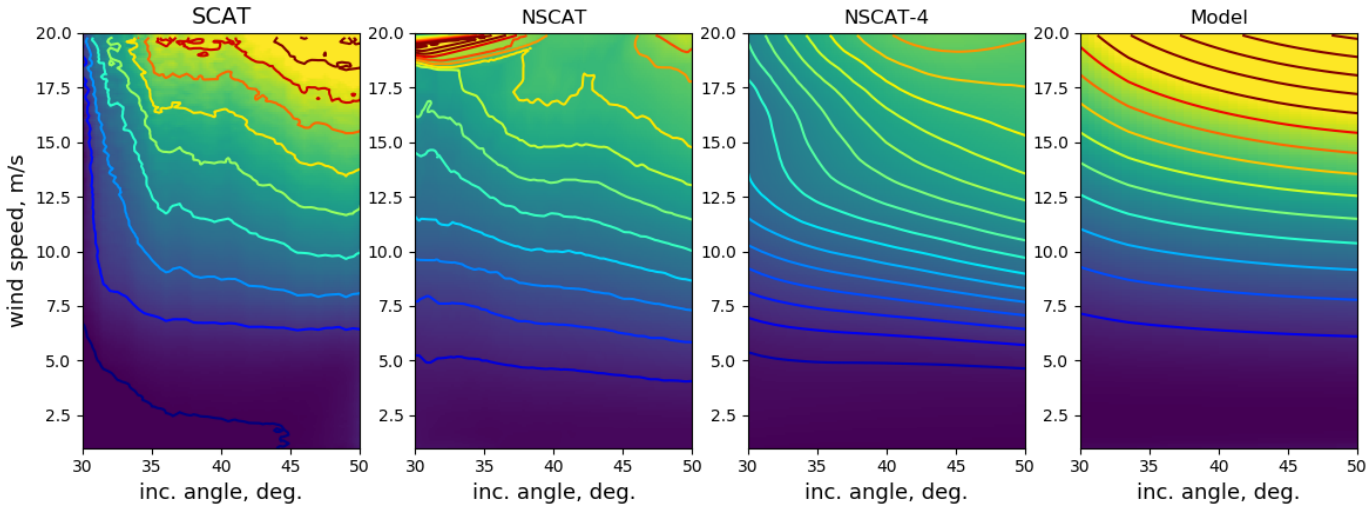

Fig. 1. Omni-directional curvature spectrum B_0 as a function of incidence angle and wind speed estimated from polarization difference obtained with different empirical GMFs and theoretical model. From left to right: SCAT forty days of global observation, NSCAT observations processed by [9], NSCAT-4 GMF [4], and model [8] estimation for microwave radar wavelength same as for SCAT instrument.

Overall, functional shapes are similar and mostly reproduced by the theoretical function. A quantitative analysis is performed for the wind exponent n in $B \propto U_{10}^n \propto \partial \ln(B_0)/\partial \ln(U_{10})$ and angular width $\delta(\theta) = A_2/A_0$ parameters. The wind exponent characterizes sensitivity to wind

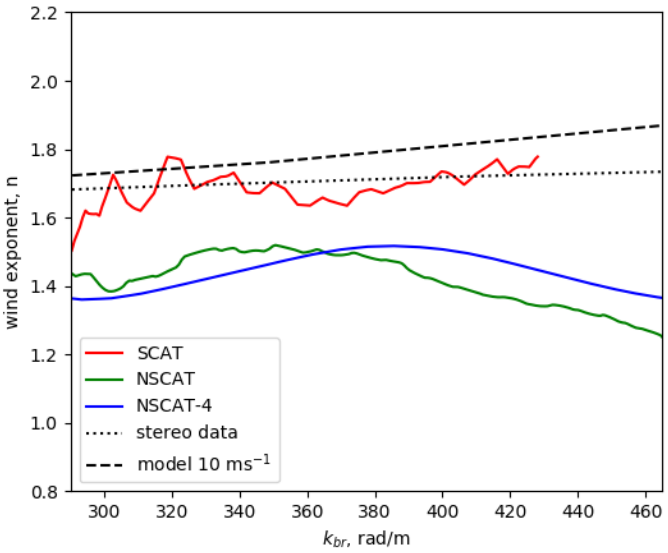

Fig. 2. Wind exponent estimated from SCAT and NSCAT observations. Dotted line corresponds to field stereo photography measurements by [7] and dashed line shows model [8] estimations at 10 m/s wind speed.

speed variations. Precise stereo-photo field measurements of this parameter were reported by [7] for a wide range of environmental conditions, and compared with actual empirical radar PD functions, see the Figure 2. Remarkably, SCAT-derived n values fully agree with photographic measurements and the model. At variance, NSCAT-GMF estimated wind exponents (both sources) show slightly smaller values. The model and in-situ experiment report an increase for n for $U_{10} < 5$ m/s. This spectral behavior is confirmed by NSCAT and SCAT measurements. Still, a larger set of low-wind observations is necessary to precise these results.

TABLE II
MODEL SENSITIVITY PARAMETERS. ALL VALUES CALCULATED FOR $\theta = 40°$ RADAR INCIDENCE ANGLE ($k_{br} = 377\,rad/m$).

	SCAT PD Model	***SCAT PD Radar***	***Photo meas. by [7]***
n, δ low winds	2.87	3.45	2.3
$3 < U_{10} < 7\,m/s$	0.50	0.42	0.4-0.6
n, δ moderate winds	1.79	1.64	1.65
$7 < U_{10} < 13\,m/s$	0.72	0.65	0.4-0.6
n, δ high winds	1.83	1.59	1.65
$13 < U_{10} < 18\,m/s$	0.72	0.50	0.4-0.6

The angular width parameter characterizes the wind direction sensitivity. From the Table II, the model and radar observations are consistent for low and moderate wind speeds. For high winds, radar-derived δ slightly decreases, while the predicted model angular width remains on the same level. This difference between the model and radar measurements may be explained by the limited growth of short capillary-gravity (1.5 cm) waves in the wind direction due to increased influence of the surface drift current on short wave dissipation, discussed in [9].

IV. Polarization Difference Model

Accordingly, the [8] spectrum exhibits a reasonable consistency with in-situ and space borne radar data. For wind inversion purposes, a PD GMF can be formulated. From the Eq. (10), (11) and (19), it writes:

$$\Delta\sigma = \Theta(\theta) B_0(\theta)\big(1 + \delta(U_{10})\cos(2\varphi)\big) \times \big(\Delta[G_{pol}^2(1 + g_{pol}s_i^2)] + \Delta[G_{pol}^2 h_{pol}]s_i^2\big]\cos\varphi\big) \quad (20)$$

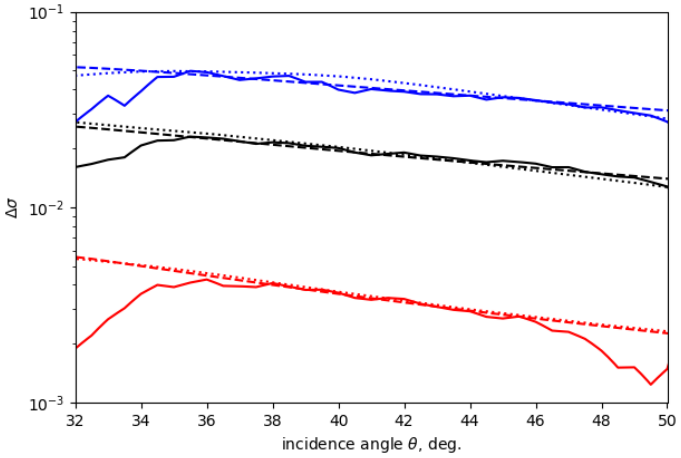

Fig. 3. The PD estimations for different Ku-band models for $U_{10} = 5$ (red), 10 (black) and 15 (blue) m/s. Dot lines correspond to NSCAT-4 ($a = 1.1$, $m = 1$), solid lines to SCAT ($a = 0.8$, $m = -1$) and dashed lines show the present model (20).

where $\Theta(\theta)$ is a calibration factor, aimed to correct antenna-gain pattern residual and instrument calibration issues. An anisotropy factor $\delta(U_{10})$ is also considered to adjust with empirical GMFs for a more realistic behavior under high wind speeds.

Figure 3 shows the comparison of SCAT and NSCAT-4 PD models with the theoretical model (20) for three different wind speeds. Here, the instrumental correction factor is expressed in a relatively simple form $\Theta = a \tan(\theta)^m$, where a adjusts the overall level of the GMF and $\tan(\theta)^m$ introduces the term related to the correction of the residual antenna gain pattern.

V. Conclusions

The PD approach can be an efficient means to more directly relate microwave measurements with sea surface wave spectral properties. As analyzed, the PD model closely reproduces the main properties of empirical radar GMFs in the range of $3 < U_{10} < 20\, m/s$. Yet, the proposed analytical framework is a physically-driven approach to more precisely include any necessary additional local environmental effects, e.g. sea surface current and temperature effects, and/or presence of biological films. This enhanced capability will thus enforce the possibility to derive a more flexible wind vector inversion, with GMF adapted to every particular geophysical situation. With this analysis, we anticipate the implementation of the proposed model to complement the existing SCAT data processor. To note, the present analysis and formulation are valid to other microwave sensing bands, and also applies to radar Doppler measurements [16], [17], to more systematically consider polarization sensitivity to improve the retrieval of ocean surface geophysical parameters, i.e. wind stress, white-caps, upper ocean currents.

Acknowledgment

This work was performed in the frame of the development of CFOSAT IFREMER Wind and Wave Operation Center (IWWOC). The IWWOC is co-funded by CNES and IFREMER. V. Kudryavtsev acknowledges the support of the Russian Science Foundation grant № 21-47-00038.

References

[1] X. Dong, D. Zhu, L. Zhang, R. Yun, W. Lin, and S. Lang, "Preliminary results of the cfosat scatterometer," in *IGARSS 2019-2019 IEEE International Geoscience and Remote Sensing Symposium*. IEEE, 2019, pp. 7881–7884.

[2] D. Hauser, C. Tourain, L. Hermozo, D. Alraddawi, L. Aouf, B. Chapron, A. Dalphinet, L. Delaye, M. Dalila, E. Dormy *et al.*, "New observations from the swim radar on-board cfosat: Instrument validation and ocean wave measurement assessment," *IEEE Transactions on Geoscience and Remote Sensing*, 2020.

[3] F. J. Wentz and D. K. Smith, "A model function for the ocean-normalized radar cross section at 14 ghz derived from nscat observations," *Journal of Geophysical Research: Oceans*, vol. 104, no. C5, pp. 11 499–11 514, 1999.

[4] "Osi saf. algorithm theoretical basis document for the osi saf wind products and nscat-4 geophysical model function," http://projects.knmi.nl/scatterometer/nscat_gmf, accessed: 2021-01-05.

[5] V. Kudryavtsev, I. Kozlov, B. Chapron, and J. Johannessen, "Quad-polarization sar features of ocean currents," *Journal of Geophysical Research: Oceans*, vol. 119, no. 9, pp. 6046–6065, 2014.

[6] V. N. Kudryavtsev, D. Hauser, G. Caudal, and B. Chapron, "A semiempirical model of the normalized radar cross-section of the sea surface 1. background model," *Journal of Geophysical Research: Oceans*, vol. 108, no. C3, 2003.

[7] M. V. Yurovskaya, V. A. Dulov, B. Chapron, and V. N. Kudryavtsev, "Directional short wind wave spectra derived from the sea surface photography," *Journal of Geophysical Research: Oceans*, vol. 118, no. 9, pp. 4380–4394, 2013.

[8] V. N. Kudryavtsev, B. Chapron, and V. K. Makin, "Impact of wind waves on the air-sea fluxes: A coupled model," *Journal of Geophysical Research: Oceans*, vol. 119, no. 2, pp. 1217–1236, 2014.

[9] Y. Quilfen, B. Chapron, A. Bentamy, J. Gourrion, T. El Fouhaily, and D. Vandemark, "Global ers 1 and 2 and nscat observations: Upwind/crosswind and upwind/downwind measurements," *Journal of Geophysical Research: Oceans*, vol. 104, no. C5, pp. 11 459–11 469, 1999.

[10] V. N. Kudryavtsev, B. Chapron, A. G. Myasoedov, F. Collard, and J. A. Johannessen, "On dual co-polarized sar measurements of the ocean surface," *IEEE Geoscience and Remote Sensing Letters*, vol. 10, no. 4, pp. 761–765, 2012.

[11] V. N. Kudryavtsev, Y. Y. Yurovsky, M. V. Yurovskaya, and B. Chapron, "Estimation of sea surface short-wave spectra from co-polarized radar backscattering cross-section," in *2017 Progress in Electromagnetics Research Symposium-Fall (PIERS-FALL)*. IEEE, 2017, pp. 2307–2314.

[12] Z. Li, A. Verhoef, and A. Stoffelen, "Cwdp top level design," https://www.nwpsaf.eu/site/download/documentation/scatterometer/cwdp/osisaf_cdop3_ss3_cwdp_top_level_design_0.9.01.pdf, 2018, accessed: 2021-01-05.

[13] J. De Vries, A. Stoffelen, and J. Beysens, "Ambiguity removal and product monitoring for seawinds," *NWP SAF report*, 2005.

[14] J. Vogelzang, "Two-dimensional variational ambiguity removal (2dvar). nwp saf nwpsaf-kn-tr-004," 2007.

[15] A. Stoffelen and M. Portabella, "On bayesian scatterometer wind inversion," *IEEE Transactions on Geoscience and Remote Sensing*, vol. 44, no. 6, pp. 1523–1533, 2006.

[16] Y. Y. Yurovsky, V. N. Kudryavtsev, S. A. Grodsky, and B. Chapron, "Ka-band dual copolarized empirical model for the sea surface radar cross section," *IEEE Transactions on Geoscience and Remote Sensing*, vol. 55, no. 3, pp. 1629–1647, 2016.

[17] Y. Y. Yurovsky, V. N. Kudryavtsev, B. Chapron, and S. A. Grodsky, "Modulation of ka-band doppler radar signals backscattered from the sea surface," *IEEE Transactions on Geoscience and Remote Sensing*, vol. 56, no. 5, pp. 2931–2948, 2018.